Nanoparticle stochastic motion in the inertial regime and hydrodynamic interactions close to a cylindrical wall

Helena Vitoshkin, Hsiu-Yu Yu, David M. Eckmann, Portonovo S. Ayyaswamy, and Ravi Radhakrishnan

Phys. Rev. Fluids **1**, 054104 — Published 28 September 2016

DOI: 10.1103/PhysRevFluids.1.054104

Nanoparticle stochastic motion in the inertial regime and hydrodynamic interactions close to a cylindrical wall

Helena Vitoshkin[a], Hsiu-Yu Yu[b], David M. Eckmann[c,d], Portonovo S. Ayyaswamy[a] and Ravi Radhakrishnan[b,c,*]

[a]Department of Mechanical Engineering and Applied Mechanics; [b]Department of Chemical and Biomolecular Engineering; [c]Department of Bioengineering; [d]Department of Anesthesiology and Critical Care, University of Pennsylvania, Philadelphia, PA, USA

[*]Corresponding author. Email: rradhak@seas.upenn.edu

Abstract

We have carried out direct numerical simulations (DNS) of the fluctuating Navier-Stokes equation together with the particle equations governing the motion of a nanosized particle or nanoparticle (NP) in a cylindrical tube. The effects of the confining boundary, its curvature, particle size, and particle density variations have all been investigated. To reveal how the nature of the temporal correlations (hydrodynamic memory) in the inertial regime is altered by the full hydrodynamic interaction due to the confining boundaries, we have employed the Arbitrary Lagrangian-Eulerian (ALE) method to determine the dynamical relaxation of a spherical NP located at various positions in the medium over a wide span of time scales compared to the fluid viscous relaxation time $\tau_\nu = a^2/\nu$, where a is the spherical particle radius and ν is the kinematic viscosity. The results show that, as compared to the behavior of a particle in regions away from the confining boundary, the velocity autocorrelation function (VACF) for a particle in the lubrication layer initially decays exponentially with a Stokes drag enhanced by a factor that is proportional to the ratio of the particle radius to the gap thickness between the particle and the wall. Independent of the particle location, beyond time scales greater than a^2/ν, the decay is always

algebraic followed by a second exponential decay (attributed to the wall curvature) that is associated with a second time scale D^2/ν, where D is the vessel diameter.

Key words: nanoparticle motion, cylindrical vessel, wall effect, hydrodynamic interaction

1. Introduction

The dynamics of nanosized Brownian particles in an unbounded fluid domain is well understood. However, in many nanotechnology applications, the evaluation of particle motion and associated transport are much more complicated since they occur in a confined geometry, arbitrarily shaped boundaries, and often in a flowing medium. For example, in nanoscale colloidal applications such as targeted drug delivery, the motion and transport associated with ligand-functionalized NPs are complicated since they occur in a blood vessel. The presence of physiological factors such as wall-hydrodynamic interactions, thermal fluctuations, and specific binding interactions between functionalizing ligands (antibodies) and cell receptors as the particle reaches the vicinity of the vessel wall will play significant roles.

Due to recent developments in nanotechnology, NP based targeted drug delivery has evinced great interest in personalized medicine, promising localized, highly potent drug therapy, with reduced side effects. Clinical optimization of drug transport within the blood vascular system and the lymphatic system requires accurate representation of NP motion in the blood stream and especially near the endothelium surface, where binding occurs between functional ligands on NPs and cell receptors. Important aspects of modeling of NP motion include consideration of Brownian dynamics, hydrodynamic and adhesive interactions mediated by molecular (receptor-ligand) binding and unbinding. Due to the dimensions of a NP, it experiences complex translational and rotational motions. This is also significantly influenced by ligand-receptor interactions. The timescales of these motions overlap with

the inertial timescale of the fluid and as such the temporal correlations in the inertial regime are strongly influenced by the confining boundaries and potentials. To comprehensively resolve the dynamics and correlations in the presence of wall-confinement, we herein carry out DNS of the fluctuating Navier-Stokes equation together with particle equations using the ALE method. We have also employed a computationally feasible deterministic method to obtain the velocity autocorrelation of fundamental interest to this investigation.

A brief summary of the known results with respect to the velocity correlations in the inertial regime, i.e., timescale $\sim a^2/\nu$, where a is the particle diameter and ν is the kinematic viscosity is provided in section A1, supplementary information (SI). The transition from exponential behavior of the velocity autocorrelation function (VACF) to algebraic behavior is attributed to influences of the fluid inertia, as shown by asymptotic analysis of the linearized hydrodynamic equations for a Newtonian fluid by Bixon and Zwanzig [1]. How the presence of a bounding planar wall alters the algebraic scaling of the VACF in the inertial regime has been analyzed by Gotoh and Kaneda [2], Pagonabarraga et al. [3], and Felderhof [4]. The latter has shown that for the parallel motion, the $t^{-1.5}$ long-time tail of the VACF components for the bulk transitions to a $t^{-2.5}$ scaling with positive amplitude in the near-wall regime, while for the perpendicular motion, a $t^{-3.5}$ scaling for the intermediate times is followed by a long-time tail that exhibits a $t^{-2.5}$ scaling with negative amplitude. Franosch and Jeney [5] have investigated the dynamics of the motion of a spherical particle near the wall by confining the particle to different distances (h) from the wall using a weak optical trap; the authors have shown that the velocity temporal correlation of the trapped particle is characterized by a $t^{-3.5}$ scaling in the bulk regime ($h/a \to \infty$) and a $t^{-4.5}$ scaling in the near-wall regime ($h/a > 1$). For a particle in the lubrication layer ($[(h-a)/a] \to 0$), only the steady translational and rotational motion has been investigated. For instance, a spherical particle moving perpendicular to the wall experiences a translational friction coefficient that is enhanced

by a factor of $a/(h-a)$ relative to ξ^{tr} [6, 7]. For rotation around the axis perpendicular to the wall, the torque coefficient is augmented by a factor of $1.2-3(\pi^2/6-1)(h/a-1)$ relative to ξ^{rot} [8, 9]. Despite all of the above efforts for particle motion under the Stokes limit, the velocity autocorrelation of a particle in the lubrication layer remains unexplored and is accomplished in the present study. The relevance and importance of transient relaxation of the NP in this regime have been recently discussed by several experimental and modeling works, see [10] for a review. While these studies have mostly focused on the adhesive energy landscape, the hydrodynamics in the lubrication regime is particularly relevant in many nanotechnology applications as well as in targeted drug delivery where the NP surface approaches the boundary separated only by receptor-ligand bonds, and the gap is of the order of ~10 nm. Results for the motion of a NP using the fluctuating hydrodynamics (FHD) approach for $t \leq a^2/\nu$ have been reported by Radhakrishnan et al. [11]. There, the adhesive interactions are modeled by harmonic springs with a spring constant k. The simulations have provided evidence of the influence of the lubrication layer on the very short timescale of NP motion. Recently, a composite generalized Langevin equation framework for the transition from the bulk to the near-wall and lubrication regimes related to a NP approaching a plane wall has been described by Yu et al. [12]. Here the memory functions of temporal hydrodynamic correlations in the bulk, intermediate, and lubrication regimes are all integrated into a composite functional. The work of Yu et. al. demonstrated that the inclusion of the harmonic potential for a NP subject to the correct memory function in the unbound state allows one to recover the correct temporal correlations in the bound state (i.e. when subject to the harmonic potential due to the spring).

While the body of work surveyed above deal with different aspects of particle motion near the wall, a detailed and consistent study of the hydrodynamic interactions in the lubrication layer and important aspects of the wall effects in the lubrication and other hydrodynamic regimes are still unavailable.

Furthermore, the majority of scaling relationships for VACF and the angular velocity autocorrelation function (AVACF) under various spatial regimes that have been obtained through the asymptotic analysis of linear hydrodynamics, their validity through direct numerical simulations of the full Navier-Stokes equation in the stochastic limit, (i.e. using the FHD method), remains to be quantified. Prior studies have primarily considered only planar boundaries, and with curved boundaries only some specific cases have been investigated [13]. The purpose of the current study is to comprehensively investigate the detailed NP hydrodynamics over relevant time scales that dictate the significance of fluid inertia, thermal motion and the presence of a curved wall.

2. Methods

Simulations have been carried out by employing the finite element method through the ALE approach [14, 15]. Here, the fluid is considered to be Newtonian and incompressible and thee governing equations are given by:

$$\nabla \cdot \mathbf{u} = 0, \tag{1}$$

$$\frac{\partial \mathbf{u}}{\partial t} + (\mathbf{u} \cdot \nabla)\mathbf{u} = \frac{1}{\rho_f}\nabla \cdot \boldsymbol{\sigma}, \tag{2}$$

$$\boldsymbol{\sigma} = -p\mathbf{J} + 2\mu\mathbf{D}[\mathbf{u}] + \mathbf{S}; \quad \mathbf{D}[\mathbf{u}] = \frac{1}{2}[\nabla\mathbf{u} + (\nabla\mathbf{u})^T], \tag{3}$$

where, $\mathbf{u}$ and ρ_f are the velocity and density of the fluid, respectively, and $\boldsymbol{\sigma}$ is the total stress tensor that includes the random stresses $\mathbf{S}$, p is the pressure, $\mathbf{J}$ is the identity tensor, $\mathbf{D}[\mathbf{u}]$ is the deformation tensor, and μ is the fluid viscosity; the random stress term is explained in subsequent discussions. The equations of motion for particle translation and rotation are described by:

$$m\frac{d\mathbf{V}}{dt} = -\int_{\partial\boldsymbol{\Sigma}_p} \boldsymbol{\sigma} \cdot \hat{\mathbf{e}}\, ds, \tag{4}$$

$$\frac{dI\boldsymbol{\omega}}{dt} = -\int_{\partial\boldsymbol{\Sigma}_p} (\mathbf{x} - \mathbf{X}) \times \boldsymbol{\sigma} \cdot \hat{\mathbf{e}}\, ds, \tag{5}$$

where $\mathbf{X}$ is the position of the centroid of the particle, $(\mathbf{x} - \mathbf{X})$ is a vector from the center of the particle to a point on its surface, $\partial\boldsymbol{\Sigma}_p$ is the particle surface, and $\hat{\mathbf{e}}$ is the unit normal vector on the surface of the particle pointing into the particle. Through the weak formulation, these terms influence the equations of fluid motion.

The simulations are performed within a cylindrical vessel with no-slip condition at the wall and particle boundaries, zero or prescribed velocity at the inlet, and a normal stress-free condition at the outlet boundary, see Figure 1:

$$\boldsymbol{V}(t=0) = \boldsymbol{V}_p, \;\; \mathbf{u}(t=0) = 0, \text{ on } \boldsymbol{\Sigma}_o - \partial\boldsymbol{\Sigma}_{in}, \tag{6}$$

$$\boldsymbol{\sigma} \cdot \hat{\mathbf{n}} = 0 \text{ on } \partial\boldsymbol{\Sigma}_{out}, \tag{7}$$

$$\mathbf{u} = \mathbf{u}_p \text{ on } \partial\boldsymbol{\Sigma}_{in}, \tag{8}$$

$$\mathbf{u} = \mathbf{V} + \boldsymbol{\omega} \times (\mathbf{x} - \mathbf{X}) \text{ on } \partial\boldsymbol{\Sigma}_p, \tag{9}$$

where $\boldsymbol{\Sigma}_o$ is the domain occupied by the fluid, and $\partial\boldsymbol{\Sigma}_{in}$ and $\partial\boldsymbol{\Sigma}_{out}$ are the inlet and outlet boundaries, respectively, $\boldsymbol{V}_p$ is the prescribed velocity of the particle (zero or random initial velocity), $\mathbf{u}_\mathrm{p}$ is the velocity of the fluid, and $\hat{\mathbf{n}}$ is the unit normal vector on the surface of the outlet wall.

The computational boundary domain is meshed using the finite element Delaunay-Voronoi method, and the fluid domain is discretized by a tetrahedralization method. Spatial discretization has been performed in such a way that volumes of elements surrounding the NP are finer (smaller) than volume element located far from the NP. Thus, in the case when the NP is located near a wall (boundary), the mesh on the wall is much finer. The generalized Galerkin weak formulation combines the fluid and the particle equations of motion using a finite element scheme for spatial discretization and a finite difference method for temporal discretization. The ALE technique has been used to resolve the mesh velocity and acceleration assuming no-slip conditions on the particle surface and smooth distribution of the nodes in

the fluid using the Laplace equation. The fluid-particle and mesh movement equations result in coupled algebraic systems which are solved iteratively at each time step via BiCG iterative solver satisfying the convergence tolerance of $\varepsilon = 10^{-9}$.

Mesh generation in ALE based finite element simulations: 4-node (vertices) and 10-node (vertices+midpoints) tetrahedrons used in the finite element representation of the computational domain and an icosahedron is used in the discretization of the spherical particle. Here l_P denotes the mesh length on the particle surface and the mesh size on the vessel wall is denoted by l_W. With the complete boundary grid information, the mesh generator next generates the elements in the interior of the domain using the Delaunay-Voronoi methods. The mesh quality is assessed by requiring the tetrahedral elements to be as regular as possible. The size and quality of the volume mesh is modified adaptively by changing the values of l_P and l_W. A finer mesh is generated by adding additional nodes to the centroid of all surface triangles that share a given node and in this process each triangle containing the given node is re-triangulated to four triangles and the corresponding mesh size changes to $l_P/2$ or $l_W/2$.

The positions of the particle and the mesh adaption are updated explicitly for each time step. The influence of Brownian motion on the behavior of the NP is considered by using FHD [15]. Since the thermal fluctuations of the surrounding fluid result in random motion, a stochastic term is additionally introduced into the stress tensor in the momentum equation of the fluid. This random stress tensor is taken to be from a Gaussian distribution, which is modeled from a Markovian noise correlation function satisfying the fluctuation-dissipation theorem. Thus, in Equation (9), the term **S** is modeled according to:

$$\langle S_{ij}(\mathbf{x}, t)\rangle = 0; \tag{10}$$

$$\langle S_{ik}(\mathbf{x}, t) S_{lm}(\mathbf{x}', t')\rangle = 2k_B T\mu(\delta_{il}\delta_{km} + \delta_{im}\delta_{kl})\delta(\mathbf{x} - \mathbf{x}')\delta(t - t'), \tag{11}$$

where δ_{ij} is the Kronecker delta, and the Dirac delta functions, $\delta(\mathbf{x} - \mathbf{x}')$ and $\delta(t - t')$, denote that the components of the random stress tensor are spatially and temporary uncorrelated. Other parameters are

chosen to be: temperature $T = 310K$, the Boltzmann constant $k_B = 1.38 \cdot 10^{-23}\, kg\, m^2/s^2K$. We have carried out simulations in the inertial regime to study the long time behavior of a spherical particle in terms of its translational and rotational VACFs. We have first considered the motion of a neutrally buoyant solid spherical NP in an incompressible Newtonian fluid with $\mu = 10^{-3}\, kg/ms$, $\rho_f = \rho_p = 10^3\, kg/m^3$ (with ρ_p being the particle density).

Figure 1 illustrates typical configurations explored in this work: a single particle of typical radius *a*=250 nm (and varied between 250 nm to 1 μm due to the relevance of this size range in pharmacological experiments) is suspended in a stationary fluid at a distance *h,* from the vessel wall. The vessel dimensions are chosen to nominally be: diameter *D* = 5 μm (and varied from 2.5 μm to 50 μm); length *L* = 10 μm (and varied from 5 μm to 25 μm) in order to mimic the representative dimensions of blood capillaries and lymph nodules. To explore the effect of the proximity to the wall on NP motion, three typical simulation setups are used: particle is located at the center of the vessel corresponding to (*h*-*a*)/*a*=9 (>1) or the bulk or core regime (Figure 1a), particle is placed near the wall, but outside the lubrication layer with (*h*-*a*)/*a* =1 or the near-wall regime (Figure 1b), and particle is inside the lubrication layer at a distance (*h*-*a*)/*a* =0.2 (<1) or the lubrication regime (Figure 1c). It should be noted that in the near-wall regime, the equations may result in a stiff system; this feature is evident from the analytical expression for the parallel component of the VACF for a particle located close to a wall, in which the series expansion of the admittance tensor contains a coefficient with a pre-factor that scales as $(h/a)^2$ [4]. In this regime, the numerical stability issues have been addressed by employing a finer mesh; i.e., the mesh density of the particle surface is doubled in comparison to the nominal value. We also note that in order to exclude computational platform dependent errors, the same calculations have been performed on servers with different hardware configurations, and the results were found to be mutually consistent.

A comparison with other methods that have reported FHD simulations can be found in Uma et al. [15]. In this context, we note that one of the strengths of our method is that due to the adaptive mesh approach, it can resolve simultaneously all three hydrodynamic regimes (see Figure 1) and satisfy still the fluctuation dissipation theorem in the FHD approach in these regimes to a high degree of statistical accuracy (see Figures A1 and A2).

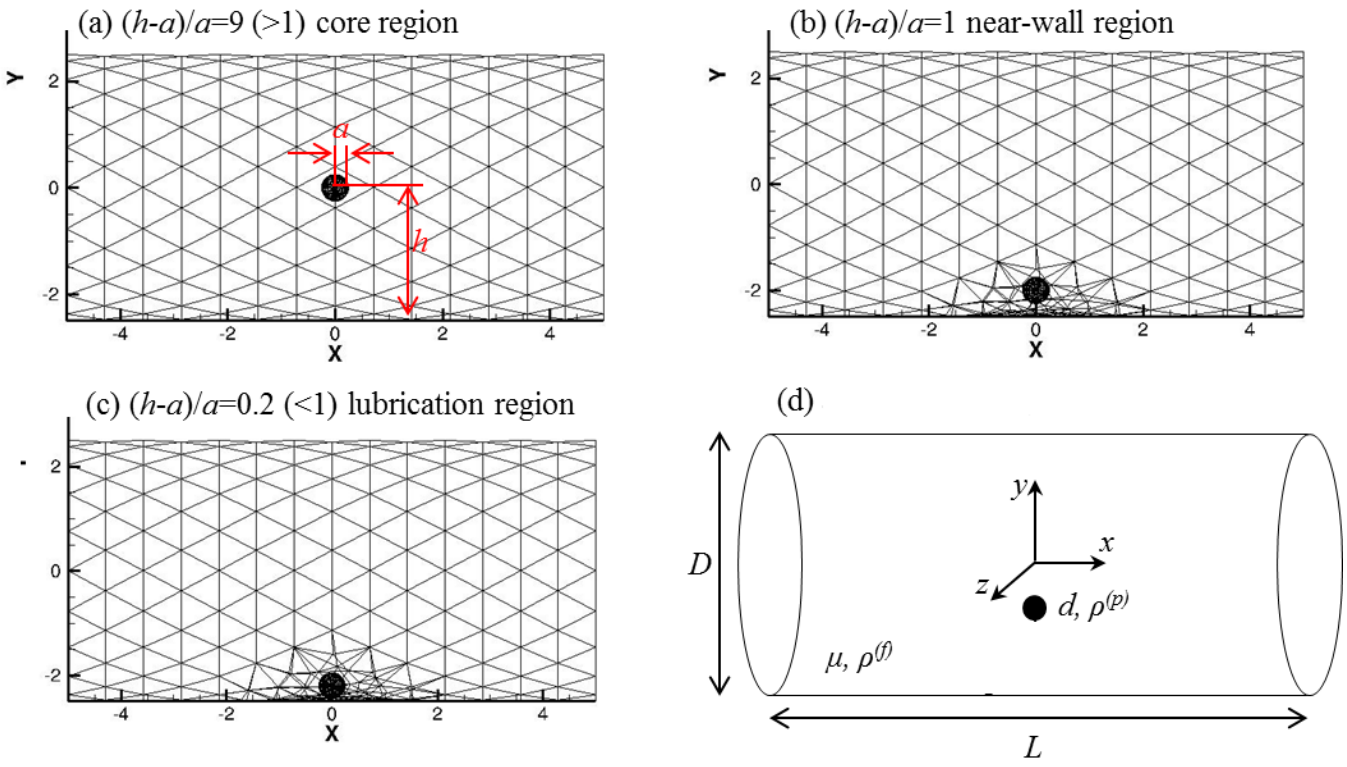

Figure 1. The surface meshes for (a) particle at the center of the vessel (bulk or core region), (b) particle located near the vessel wall (near-wall region), and (c) particle in the lubrication layer (lubrication region). (d) Schematic view of a NP in a cylindrical vessel.

In order to determine the appropriate time step, , for computation, we first examine the various relevant time scales. For the dynamics of a particle in a stationary fluid within a vessel, there are three

relevant fluid time scales: (i) the hydrodynamic time scale or viscous dissipation time, $\tau_\nu = a^2/\nu$; (ii) the momentum diffusion time in a cylindrical vessel geometry, $\tau_D = D^2/\nu$, which is the time required for a disturbance emitted from near the particle surface to reach the vessel wall; and, (iii) the time scale of sound propagation in experiment (or a real fluid) over a distance equal to the radius of the particle, $\tau_c = a/c$, where c is the speed of sound. In our case of interest c_{blood} is approximately $1540\ m/s$ [16]. In the present simulation, for a nanoparticle (NP) of radius $= 250\ nm$, these timescales are $\tau_\nu = 6.25 \cdot 10^{-8}s$, $\tau_D = 2.5 \cdot 10^{-5}s$ and $\tau_c = 1.6 \cdot 10^{-10}s$. The importance of sound propagation is defined by the compressibility factor, $\tau_c/\tau_\nu = 0.003$, which is small enough to justify the assumption of fluid incompressibility within the considered timescales. Furthermore, for the Brownian motion of the particle, the Brownian relaxation time, $\tau_b = m/6\pi\mu a = 1.38 \cdot 10^{-8}s$. On the basis of these estimates, the time step has been chosen satisfying the requirement that $\Delta t \ll \tau_b, \tau_\nu$; we note that an additional timescale of $\tau_{gap} = (h-a)^2/\nu$ arises in our simulation. Observe that $\tau_b < \tau_\nu$ and it is the most stringent time scale. Based on our numerical experimentation, we note that for FHD simulations, it is preferable to have a Δt less than two orders of magnitude compared to τ_b, while for deterministic simulations where the Brownian dynamics is not considered, it is sufficient to take $\Delta t < \tau_\nu$. Therefore, we have chosen for FHD simulations $\Delta t^{FHD} = 10^{-10}$s and for deterministic simulations $\Delta t^{det} = 10^{-9}$s; these values are also less than τ_{gap} for all the values of h investigated in this study. The number of simulation steps has been chosen as $N \geq 10^5$ thus allowing for exploring the longtime decay of the VACFs. After considerable numerical experimentation, the time convergence criterion was estimated as $\|t^{k+1} - t^k\| < 10^{-7}$.

3. Method Validation

We begin by establishing the equilibrium characteristics of the simulations in terms of the temperature

and the probability distributions of the translational and rotational velocities of a spherical NP, which is initially placed in one of the three locations in a cylindrical vessel containing a stationary fluid: at the center, near the wall, and in the lubrication layer, see Figure 1. We first verified that the FHD approach yields the correct temperature, as well as the equilibrium distribution for velocities and angular velocities in all hydrodynamic regimes to within a statistical error of <5%, see section A2 and Figure A1 in SI. The results imply that the system adheres to thermal equipartition in all hydrodynamic regimes considered in Figure 1, thereby validating the numerical procedure and the choice of mesh resolution. While other approaches to FHD such as the fluctuating Lattice-Boltzmann technique or the immersed boundary technique have been reported in the literature, see references discussed in Uma et. al. [15], we note that the adherence of equipartition across all hydrodynamic regimes for both translational and rotational motion is uniquely achieved by the ALE method described here.

After the successful characterization of thermal equipartition, we proceed to calculate the VACFs of the spherical particle. Figure A2 in SI shows the translational and rotational VACFs for the three velocity components. Twenty-five realizations have been harvested for each simulation setup in order to achieve temperature equilibration and to reduce the statistical error in the VACFs. The data from 25 realizations are averaged during post-processing and the error bars depict the standard deviation of the VACFs obtained with 25 realizations. Despite the averaging over multiple trajectories, for later times ($t > \tau_\nu$ for translation, and $t > 0.2\tau_\nu$ for rotation) in Figure A2, the FHD results show significant statistical error. In principle, this error can be reduced by averaging over more realizations or by increasing the time of integration for each sampled trajectory. However, this would lead to an onerous computational overhead. An alternative and effective way to study the long time behavior of the VACF in a stationary medium is the consideration of the motion of a particle, which is initially driven by an external impulsive force yielding a $V(0)$, and omitting the consideration of the subsequent random thermal stresses, which we

term the deterministic method. According to the fluctuation-dissipation theorem, the time correlation of the thermal stresses is inherently equal to the temporal correlation of the hydrodynamic memory of the stationary fluid [17]. The equivalence of the deterministic and FHD approaches is explicitly derived in section A3 in SI; the deterministic approach is also adopted in previous simulations of Ref. [3, 18], and [12], and in the theoretical derivation of Ref. [4].

In Figure A2, we provide short time ($t < \tau_\nu$) analyses of translational (a,c,e) and rotational (b,d,f) velocity components of a neutrally buoyant particle of $d=2a$=500 nm diameter suspended in a vessel of D = 5 μm diameter in a stationary fluid medium. The agreement of the deterministic method with the stochastic method, as well as the consistency with the analytical expressions for asymptotic scaling with respect to temporal correlations in the short time-scale in multiple hydrodynamic regimes (summarized in Figure 1, main text) are taken as successful validation of our formalism and numerical procedures with respect to the correct reproduction of temporal correlations in the short time-scale.

4. Results and discussion

4.1. *Long time behavior of the VACF in the inertial regime and the effect of a curved wall*

Long-time behavior of the velocity (or the VACF) in the inertial regime for a particle at different locations relative to the boundary is analyzed together with the effect of the wall curvature on the motion of the particle are displayed in Figure 2 for the translational velocity components; the corresponding results for the rotational velocity components are provided in Figure A3. Due to the excellent agreement between the FHD and the deterministic results discussed above, we have now carried out the evaluations using the deterministic method which resolves the longer time behavior without being clouded by statistical noise caused by thermal fluctuations. In order to elucidate the effects of the wall curvature as well as the confinement due to the cylindrical tube, we compare our

results for the long-time scaling for the VACF with the analytical expressions of Hauge and Martin-Lof [19] for a particle in an unbounded domain, and Felderhof [4] and Franosch and Jeney [5] for a particle close to an infinite planar wall. To comprehensively examine this effect, we have performed the calculations on systems with increasing vessel diameters: D/d=10, 20, 40 and 100; $D/d\rightarrow\infty$ represents the limit of the infinite planar wall. Also, we have carried out a particle-size scaling analysis by choosing different particle diameters, d=250, 500, and 1000 nm, while keeping the ratios (D/d) and ((h-a)/a) the same for these different cases. Our results are not altered by the particle size for the parameter range examined here; see section A4 and Figure A4 in SI. We also examine how our results are sensitive to changing the vessel length. It is found that for the range of L=D to L=3D the results are essentially independent of the tube length; see section A5 and Figure A5 in SI. Finally, the effect of particle density on VACF is summarized in section A6 (and Figure A6) in SI.

Apart from the short-time exponential decay and the intermediate-time algebraic decay noted in Figure A2, we observe that at much longer times, $t > C_1^{tr}\tau_D$ or $C_1^{rot}\tau_D$ with $\tau_D = D^2/\nu$, a second exponential decay ($\exp(-C_2^{tr}t/\tau_D)$ or $\exp(-C_2^{rot}t/\tau_D)$ with pre-factors $C_2^{tr}$and C_2^{rot}). In this context, we note that the long-time exponential decay of the parallel component of the VACF in a medium bounded by two parallel plates was shown using the mode coupling approach [20]. Frydel and Rice [21] have analytically examined the dynamics of a spherical particle suspended in a fluid confined by two parallel walls for a quasi-two-dimensional motion. It is shown that, for no slip boundary conditions, the long-time VACFs for both parallel and perpendicular motions obey an exponential decay with a friction coefficient $\xi \propto \pi^2\upsilon/H^2$, where H is the separation between two walls. Tatsumi and Yamamoto [22] have studied the velocity relaxation of a spherical particle subject to an impulse and confined between two parallel planar walls. Their results show that the long-time decay of the velocity parallel to the walls is proportional to $t^{-5/2}\exp(-\upsilon\pi^2 t/H^2)$, which is attributed to a continuous spectrum of viscous modes

with wave vector components perpendicular to the walls with a magnitude of π/H. For a cylindrical geometry, in the insets of Figures 2a and A3a for different D/d, we compare the time scale at which the second exponential decay appears, where the particle velocity deviates from the algebraic scaling at least by 10%. Not surprisingly, this characteristic time is found to be only a function of D/d or τ_D/τ_v. Our observations of the long-time exponential correlation show similar trends to the results reported in the literature cited above, thus supporting the argument that the long-time exponential decay seen in our velocity relaxation is a signature of the strong confinement due to the bounding curved wall.

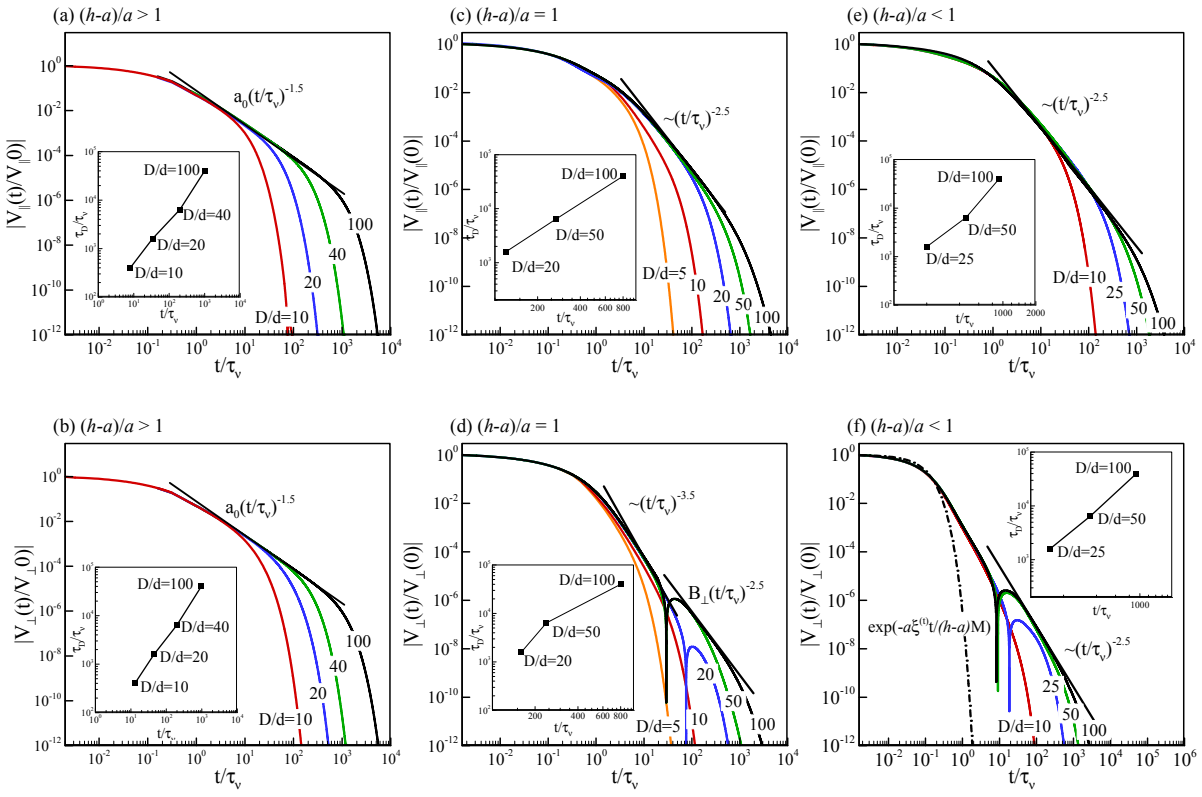

Figure 2. The effect of confinement and curvature of the cylindrical wall on the translational velocity of a 500 nm-diameter particle in a stationary fluid (calculated by the deterministic method), located in the center of the vessel with (a) parallel (axial) and (b) perpendicular (radial) directions; near wall in a

direction (c) parallel, (d) perpendicular to the wall, and (e) parallel, (f) perpendicular in the lubrication zone. Constants for the power-law scaling are [5]: $a_0 = 1/6\sqrt{\pi}$ (see section A1) and $B_\perp = (h^2/a^2 - 5/9)/4\sqrt{\pi}$. The inset in each panel shows the corresponding comparison between τ_D and the time at which the second exponential decay appears ($\sim C_1^{tr}\tau_D$; see discussion in text). The coefficient C_1^{tr} are approximately 0.025, 0.017, and 0.019 for bulk, near-wall, and lubrication regimes, respectively. We note that the coefficients were determined by plotting the axes in a semi-log scale and then fitting the data.

We perform similar analysis for a particle located in the near-wall regime, i.e. (*h*-*a*)/*a*=1. The parallel /perpendicular components are illustrated in Figure 2c/2d for translational and Figure A3c/A3d for rotational velocities. The results for the translational motion show that, for *D*/*d*<20, the velocity decays exponentially without a clear intermediate algebraic scaling. For larger diameters, after the initial Stokes-exponential decay, algebraic correlations are observed, where the parallel motion displays a $t^{-2.5}$ scaling and the perpendicular motion first displays a $t^{-3.5}$ scaling behavior at intermediate times ($t \sim h^2/\nu$) followed by a $t^{-2.5}$ scaling with a negative sign (anticorrelation) due to the wall reflection of the diffused vortex. These temporal correlations show the same trend as those predicted by Felderhof [4] and Franosch and Jeney [5] for a particle close to a planar wall. Eventually, the algebraic decay transitions to a final exponential decay due to the wall confinement. Figure 2d also illustrates that the presence of a curved wall causes an anticorrelation to occur at later times compared to those for a particle near a planar wall [4]. Similar trends are observed for the angular velocity relaxation where it first shows an initial exponential decay characterized by the instantaneous Stokes drag followed by an algebraic decay ($t^{-2.5}$ scaling for rotation about the parallel axis and $t^{-3.5}$ for perpendicular axis [3]) and a

long-time, second exponential decay. However, the anticorrelation due to the reflection of the fluid vorticity is observed only for rotation about the parallel axis, as shown in Figure A3c.

In Figures 2e,f and A3e,f, we depict the time evolution of the velocity for a particle in the lubrication layer, or (h-a)/a<1. The general characteristics of the velocity temporal response are similar to those for the near-wall case. However, the enhanced Stokes drag for the lubrication layer leads to a more distinct separation between the two exponential decays such that the intermediate algebraic decay is manifest even for smaller vessel diameters. We again observe that for $V_{\perp}$ the anticorrelation in the smaller vessel occurs at later times, indicating that the vessel curvature constrains the evolution of the particle motion. Eventually, the algebraic decay changes to a final exponential correlation due to the presence of strong confinement of the vessel wall. The angular velocity relaxation about the parallel axis exhibits the same general trend as in the near-wall case where the anticorrelation is noted to occur at later time scales for smaller tube diameters. In the lubrication regime this effect is significant for rotation about the perpendicular axis such that anticorrelation is observed (compare Figure A3d and Figure A3f).

In Figure 3, we present the pre-factor C_2 of the long-time exponential decay for all the cases investigated. We observe that for both translational and rotational velocity components, C_2 is only weakly dependent on the tube diameters for small tubes (D/d <40) and is almost independent of $(h-a)/a$. This finding suggests that: (1) the curved bounding wall would lead to a greater degree of reflection of the fluid momentum from the boundary compared to a planar wall, irrespective of the particle location, and (2) over long times, this faster decay is governed by the characteristic size of the confinement, i.e. the tube diameter.

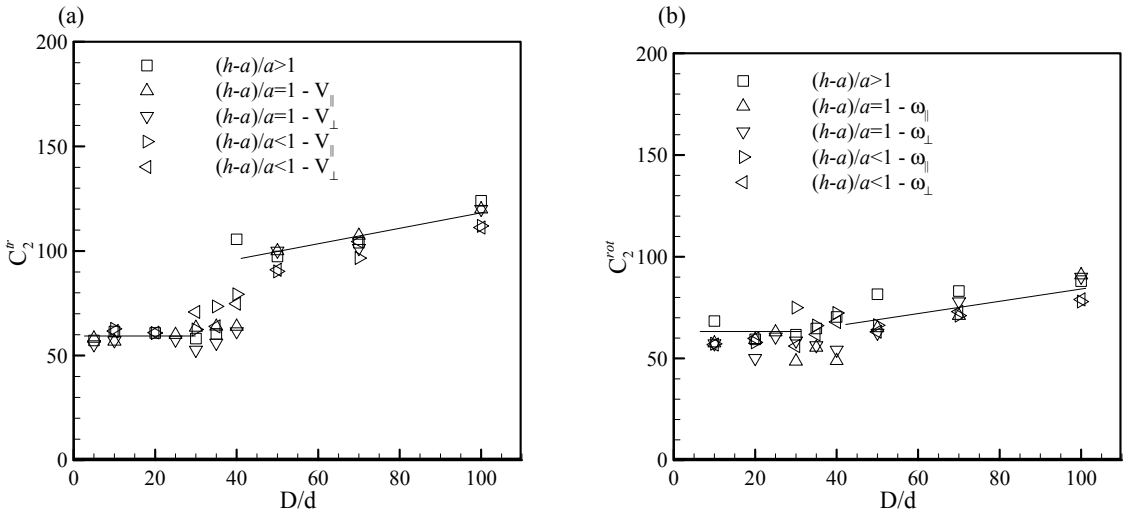

Figure 3. The pre-factor of the second exponential decay, $\exp(-C_2^{tr}t/\tau_D)$ and $\exp(-C_2^{rot}t/\tau_D)$, for (a) translational and (b) rotational velocities with different vessel diameters and hydrodynamic regimes.

To summarize the result presented in Figures 2,3 (and Figure A3), we conclude that the VACF exhibits an initial exponential decay $e^{-\beta\xi t/M}$ with β characterizing the enhanced drag (e.g., for translational motion $\beta = 1$ in the bulk, $\beta_{\parallel} = 1/(1 - 9a/16h)$ and $\beta_{\perp} = \frac{1}{\left(1-\frac{9a}{8}h\right)}$ for the near-wall regime, and $\beta_{\parallel} = (8/15)\,ln((h-a)/a) - 0.9588$ and $\beta_{\perp} = a/(h-a$ for the lubrication regime) followed by an expected algebraic decay ($t^{-1.5}$ for bulk, $t^{-2.5}$ for near-wall and lubrication regimes). Eventually, a second exponential decay occurs at the time scale $\sim\tau_D$ independent of the hydrodynamic regime, characterizing the long-time behavior of the VACF shaped by the confining wall. The wall curvature influences the onset timescale for the $t^{-2.5}$ scaling.

4.2. Time-dependent diffusivity and the effect of a curved wall

We utilize the computed temporal correlations of the velocity and evaluate the normalized time-dependent diffusivity using the following relation,

$$D(t)/D_{bulk} = {D_{bulk}}^{-1} \int_0^t \langle V(t')V(0)\rangle dt' = (6\pi\mu a/M) \int_0^t [V(t')/V(0)]dt', \quad (14)$$

where $D_{bulk} = k_B T/6\pi\mu a$ is the Stokes-Einstein diffusivity for a particle in an infinite fluid domain. As can be seen from Figures 4a and 4b for the translational motion, the diffusivity gradually approaches to a steady-state, long-time value for both parallel and perpendicular directions. The long-time diffusivity agrees closely with the results calculated from the mean-squared displacement of the particle using the FHD approach (dashed lines) [15], with slight deviations due to statistical noise inherent in a FHD approach. It is noteworthy that both $D_{\parallel}$ and $D_{\perp}$ have a faster transition to the long-time value if h/a or $(h-a)/a$ is smaller, as the VACFs also exhibit faster decay. In Figure 4c, we compare the value of diffusivity at the viscous relaxation time (τ_ν) with its long-time value for different hydrodynamic regimes. We find that in the lubrication layer, ((*h*-*a*)/*a*<1), the particle moving perpendicular to a wall exhibits long-time diffusive behavior even before the fluid momentum diffuses over the particle size. This result is consistent with the NP experiencing the enhanced stokes drag, which significantly reduces the relaxation time. Therefore, the NP diffusion could compete more effectively with molecular-level relaxations such as binding unbinding kinetics between the ligand on the NP surface and the receptor on the cell surface, a concept that has been invoked in a previous study [12].

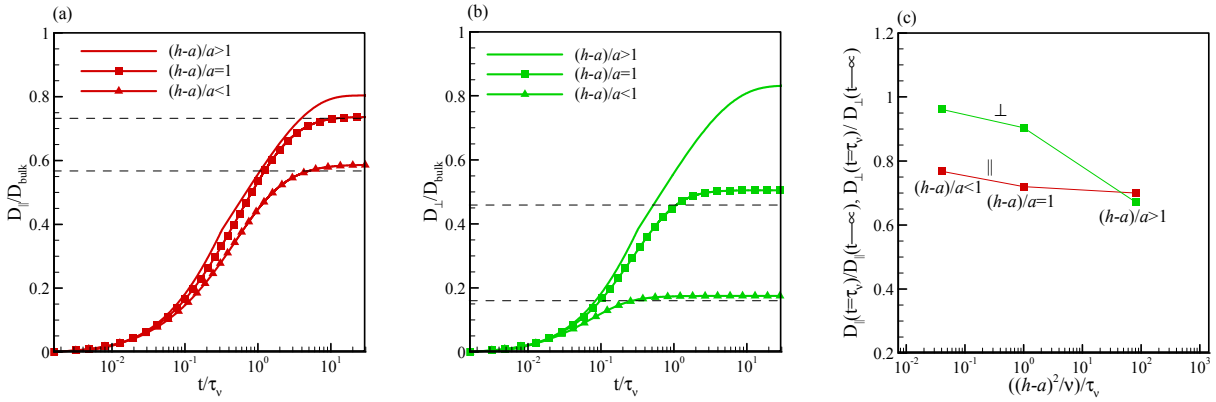

Figure 4. Time dependent diffusivity for (a) parallel and (b) perpendicular motions normalized by the Stokes-Einstein diffusivity for a particle in an unbounded medium, $D_{bulk} = k_B T/6\pi\mu a$. Three different particle positions (hydrodynamic regimes) are compared, and $D/d = 10$. Dashed lines represent the results calculated by [15] using the FHD approach. (c) The ratio of the diffusivity at $t = \tau_\nu$ to that at $t \to \infty$ as a function of h^2/a^2 for both parallel and perpendicular components are shown in (a) and (b).

5. Conclusions

The dynamics of a neutrally-buoyant or a nearly neutrally-buoyant Brownian NP in an incompressible stationary fluid medium contained in a cylindrical vessel is comprehensively studied using the FHD approach as well as an equivalent deterministic approach based on DNS of ALE Galerkin finite element method. The translational and rotational motions of a NP located in various positions (i.e. center of the vessel, near-wall, and the lubrication region) in a quiescent fluid was explored. It is found that the simulation of the Brownian motion using FHD is feasible for times comparable with the fluid viscous dissipation time, beyond which the computational overhead becomes formidable. However, the long-time velocity relaxation can be accurately calculated using the deterministic method where an impulsive random force is applied to the particle and the subsequent discerned without regard to thermal

fluctuations. The VACFs and AVACFs for different hydrodynamic regimes are compared with published results, where possible; the close agreement in the bulk and the near-wall regimes validate our numerical studies. New results in this study demonstrate a systematic approach for studying the temporal hydrodynamic correlations in the presence of a curved vessel wall, particle size, particle-fluid density variations especially focusing on the lubrication regime. In summary, when the particle is in a stationary fluid, the cylindrical confinement yields a second exponential correlation following the intermediate-time algebraic decay seen in the VACF. The wall curvature not only affects the onset and the time constant of the exponential correlation, but also alters the time scale for the anticorrelation caused by the wall boundary. We show that small variations of particle density relative to the fluid density only impact the relaxation of the perpendicular component for the translational motion when the particle is near the wall and in the lubrication layer.

The significance of our study in terms of capturing the VACF of NP motion under a variety of confinement and flow conditions can be recognized in relation to the generalized Langevin equation (GLE) formalism for NP motion [12, 23, 24]. GLE is a mathematical construct for the particle equation of motion that incorporates a memory function denoting a systematic resistance and a complementary random fluctuating force. While GLE for a Brownian particle near a boundary can be formulated from the Mori-Zwanzig projection formalism [25], the main complexity originates from the fact that different hydrodynamic modes correlate at different time scales, especially when boundaries, confining potentials, and flow-fields are introduced. In such circumstances, the VACF determined by DNS provide a direct input to the GLE by defining the memory function. Thus, the VACF determined through a DNS approach can be regarded as a crucial component of temporal modeling in the inertial regime, wherein the DNS approach presented here provides the short-to-intermediate timescales of the memory function. This approach can be gainfully employed in several applications involving colloidal systems in

nanotechnology, where the nanoscale architecture of disordered and ordered matrices may have a significant bearing on interaction and passage of functional nanoparticles and assembled nanomaterials such as in a living tissue. In such circumstances, the combination of DNS and GLE can be used to describe the temporal dynamics and elucidate the governing principles for the driving forces as a function of the nature/structure of the confinement. As a logical extension of this work, we envision that such future studies can significantly impact the design of functional nanomaterials with applications in targeted drug delivery and regenerative medicine.

Acknowledgments

The fluctuating hydrodynamics aspects of this work was supported in part by the National Institutes of Health (NIH) grant R01 EB006818 and the deterministic direct numerical simulations aspects were partially supported by NIH U01 EB016027. We acknowledge shared computational resources provided by XSEDE (Grant No. MCB060006) and NSF DMR 1120901.

References

1. Zwanzig, R. and M. Bixon, *Hydrodynamic Theory of the Velocity Correlation Function.* Physical Review A, 1970. **2**(5): p. 2005-2012.
2. Gotoh, T. and Y. Kaneda, *Effect of an infinite plane wall on the motion of a spherical Brownian particle.* The Journal of Chemical Physics, 1982. **76**(6): p. 3193-3197.
3. Pagonabarraga, I., et al., *Algebraic decay of velocity fluctuations near a wall.* Physical Review E, 1998. **58**(6): p. 7288-7295.
4. Felderhof, B.U., *Effect of the Wall on the Velocity Autocorrelation Function and Long-Time Tail of Brownian Motion†.* The Journal of Physical Chemistry B, 2005. **109**(45): p. 21406-21412.
5. Franosch, T. and S. Jeney, *Persistent correlation of constrained colloidal motion.* Physical Review E, 2009. **79**(3): p. 031402.
6. Cox, R.G. and H. Brenner, *Slow Motion of a Sphere through a Viscous Fluid Towards a Plane Surface .2. Small 99gap Widths Including Inertial Effects.* Chemical Engineering Science, 1967. **22**(12): p. 1753-&.
7. Leal, L.G., *Advanced transport phenomena: fluid mechanics and convective transport processes*. 2007: Cambridge University Press.

8. Jeffery, G., *On the steady rotation of a solid of revolution in a viscous fluid.* Proceedings of the London Mathematical Society, 1915. **2**(1): p. 327-338.
9. Goldman, A.J., R.G. Cox, and H. Brenner, *Slow viscous motion of a sphere parallel to a plane wall—I Motion through a quiescent fluid.* Chemical Engineering Science, 1967. **22**(4): p. 637-651.
10. Ayyaswamy, P.S., et al., *Nanocarrier Hydrodynamics and Binding in Targeted Drug Delivery: Challenges in Numerical Modeling and Experimental Validation.* J Nanotechnol Eng Med, 2013. **4**(1): p. 101011-1010115.
11. Radhakrishnan, R., et al., *Temporal multiscale approach for nanocarrier motion with simultaneous adhesion and hydrodynamic interactions in targeted drug delivery.* Journal of Computational Physics, 2013. **244**(0): p. 252-263.
12. Yu, H.-Y., et al., *Composite generalized Langevin equation for Brownian motion in different hydrodynamic and adhesion regimes.* Physical Review E, 2015. **91**(5): p. 052303.
13. Felderhof, B.U., *Transient flow of a viscous incompressible fluid in a circular tube after a sudden point impulse.* Journal of Fluid Mechanics, 2009. **637**: p. 285-303.
14. Hu, H.H., N.A. Patankar, and M.Y. Zhu, *Direct Numerical Simulations of Fluid–Solid Systems Using the Arbitrary Lagrangian–Eulerian Technique.* Journal of Computational Physics, 2001. **169**(2): p. 427-462.
15. Uma, B., et al., *Nanoparticle Brownian motion and hydrodynamic interactions in the presence of flow fields.* Physics of Fluids, 2011. **23**(7): p. 073602.
16. Duck, F.A., *Chapter 4 - Acoustic Properties of Tissue at Ultrasonic Frequencies*, in *Physical Properties of Tissues*, F.A. Duck, Editor. 1990, Academic Press: London. p. 73-135.
17. Kubo, R., *The fluctuation-dissipation theorem.* Reports on progress in physics, 1966. **29**(1): p. 255.
18. Iwashita, T., Y. Nakayama, and R. Yamamoto, *A Numerical Model for Brownian Particles Fluctuating in Incompressible Fluids.* Journal of the Physical Society of Japan, 2008. **77**(7): p. 074007.
19. Hauge, E.H. and A. Martin-Löf, *Fluctuating hydrodynamics and Brownian motion.* Journal of Statistical Physics, 1973. **7**(3): p. 259-281.
20. Bocquet, L. and J.-L. Barrat, *Hydrodynamic properties of confined fluids.* Journal of Physics: Condensed Matter, 1996. **8**(47): p. 9297.
21. Frydel, D. and S.A. Rice, *Hydrodynamic description of the long-time tails of the linear and rotational velocity autocorrelation functions of a particle in a confined geometry.* Physical Review E, 2007. **76**(6): p. 061404.
22. Tatsumi, R. and R. Yamamoto, *Velocity relaxation of a particle in a confined compressible fluid.* The Journal of Chemical Physics, 2013. **138**(18): p. 184905.
23. Balakrishnan, U., et al., *Generalized Langevin dynamics of a nanoparticle using a finite element approach: Thermostating with correlated noise.* 2011.
24. Uma, B., et al., *A hybrid formalism combining fluctuating hydrodynamics and generalized Langevin dynamics for the simulation of nanoparticle thermal motion in an incompressible fluid medium.* Molecular physics, 2012. **110**(11-12): p. 1057-1067.
25. Hansen, J.-P. and I.R. McDonald, *Theory of Simple Liquids: With Applications to Soft Matter*. 2013: Academic Press.